ADVANCES IN ATMOSPHERIC SCIENCES, VOL. 29, NO. 1, 2012, 54–??

Implication of the South China Sea Throughflow for the Interannual Variability of the Regional Upper-Ocean Heat Content

LIU Qinyan*[1] (刘钦燕), Ruixin HUANG[2], and WANG Dongxiao[1] (王东晓)

[1]*State Key Laboratory of Tropical Oceanography, South China Sea Institute of Oceanology, Chinese Academy of Sciences, Guangzhou* 510301

[2]*Deptartment of Physical Oceanography, Woods Hole Oceanographic Institution, Woods Hole, Massachusetts* 02543, *USA*

(Received 1 November 2010; revised 23 March 2011)

ABSTRACT

In this study the interannual variability of the upper-ocean heat content in the South China Sea (SCS) was revisited using simple ocean data assimilation (SODA) combined with objective analyzed data sets that included the horizontal and vertical structures. The results confirmed that the upper-ocean heat content in the SCS is lower than normal during the mature phase of El Niño events, and two super El Niño events, 1982/1983 and 1997/1998 were also included. The variability of the heat content was consistent with the variability of the dynamic height anomalies. The SCS throughflow (SCSTF) plays an important role in regulating the interannual variability of the heat content, especially during the mature phase of El Niño events.

Key words: heat content, South China Sea throughflow

Citation: Liu, Q. Y., R. X. Huang, and D. X. Wang, 2012: Implication of the South China Sea throughflow for the interannual variability of the regional upper-ocean heat content. *Adv. Atmos. Sci.*, **29**(1), 54–62, doi: 10.1007/s00376-011-0068-x.

1. Introduction

The ocean circulation and water properties in the South China Sea (SCS) are regulated by the atmospheric forcing and by the mass exchanges of water with the adjacent oceans. In particular, circulation in the northern SCS is regulated by water exchange between the SCS and the western Pacific (e.g., **?**; **?**; **?**). The Luzon Strait Through flow (LST) carries the El Niño and Southern Oscillation (ENSO) signals into the SCS, working as an oceanic bridge and playing an important role in regulating the circulation and heat budget in the SCS (**?**). Of course, changes in local wind forcing in the SCS, connected to ENSO through the atmospheric bridge, may play another important role in regulating the interannual variability of circulation in the SCS (**?**). After the Pacific water enters the SCS, part of it returns to the Pacific through the Kalimantan and the Makassar straits, thus affecting the variability of the Indonesian Throughflwo (ITF) (**?**; **?**; **?**; **?**).

The SCS throughflow (SCSTF) involves the inflow through the Luzon Strait and the outflow through the Karimata, Mindoro, and Taiwan straits (**?**). The Luzon Strait transport (hereafter, LST) is the dominant branch of the SCS throughflow (SCSTF), and it has attracted much attention recently (e.g., **?**; **?**; **?**, 2008; **?**; **?**, 2010).

During El Niño events, the horizontal heat advection associated with the LST plays an important role in regulating heat storage in the SCS (**?**), and this Pacific-water pathway through the SCS has a notable impact on heat transfer in the Indonesian throughflow (**?**). The SCSTF is a conveyor belt transferring up to

*Corresponding author: LIU Qinyan, qyliu66@scsio.ac.cn

0.2 PW (1 PW=10^{15} W) of heat and 0.1 Sv (1 Sv=10^6 m^3 s^{-1}) of freshwater from the SCS into the Indonesian maritime continent. On the other hand, SCS acts as a heat capacitor, storing heat in certain years and releasing it in others (**?**). The importance of the SCSTF to the climate variability of the Indo-Pacific region has also been confirmed by numerical experiments (e.g., **?**, 2009; **?**). The dynamic role played by the SCSTF also has been identified through subsurface salinity distribution (**?**), and **?** recently reviewed the related studies on the SCSTF, including its dynamics, variability and application for climate.

The cooling role played by the SCSTF during El Niño events had been reported by Qu et al. (2006). But in their study, the cooling effect played by the SCSTF did not take place during 1982/1983 and 1997/1998. In this study, we used the different data sets to further report our understanding of the interannual variations of the upper-ocean heat content (HC) in the SCS and the role played by ocean advection. Our results show that the cooling effect played by the SCSTF on the upper-ocean HC can also take place during these two typical El Niño events, 1982/1983 and 1997/1998, which is different from that reported by **?**.

2. Data and methods

Monthly Simple Ocean Data Assimilation (SODA) data sets were used in this study (**?**); they contained two subsets of data of the Ocean General Circulation Modeling (OGCM) results, each using different sets of wind forcing. The first data set was the OGCM result forced by European Center for Medium Range Weather Forecasts (ECMWF) reanalysis winds for the period 1958–2001 (SODA_2.0.2); the second data set comprised the results obtained from OGCM forced by QuikSCAT winds for the period 2002–2007 (SODA_2.0.4). The total time length covered by these two data sets was 50 years. SODA is a global model that includes meridional direction [south of 75.25°S is land (Antarctica)]. The model has a horizontal resolution of 0.5°×0.5° and 40 levels in the vertical direction with the 10-m vertical spacing at the sea surface and increasing to 100–250 m at depth below 1000 m.

The HC in the upper 465 m was calculated using SODA products as follows:

$$\mathrm{HC}_{i,j} = \int_{-465}^{0} \rho c_p T_{i,j,z} A_{i,j} dz$$

where $\rho = 1024$ kg m^{-3} is the mean water density at as the sea surface, $c_p = 4007$ J kg^{-1} K^{-1} is the specific heat at constant pressure, $T_{i,j}$ is temperature, and $A_{i,j}$ is the horizontal area of the given 0.5°×0.5° grid box.

In addition, to reflect the subsurface variability associated with thermocline dynamics variation, the dynamic height (DH) product estimated from objectively analyzed monthly mean temperature and climatological salinity was used in this study, with a reference level of 700 m (**?**)[a]. To discuss the process of generating the SCS HC anomalies, the ECMWF ERA40 surface heat flux obtained from the ECMWF Data Server was also used in section 3.

3. Results

3.1 *The relationship between upper-ocean HC and El Niño*

The raw and interannual variability of the NINO3.4 Index and the domain-integrated HC in SCS are shown in Fig. 1. If no special illustrations are given, the correlation coefficients obtained were based on the smoothed time series. The domain covered the region with water depth >100 m (see Fig. 4). The maximum correlation coefficient was −0.41 when the modeled HC led the NINO3.4 index for 4 months, and it reached −0.46 when the DH led the NINO3.4 index for 2 months. The upper-ocean HC estimated from SODA products and DH estimated from objectively analyzed temperature shared similar interannual variability ($r = 0.59$, Figs. 1b and c)[b]. On interannual time scales, the upper-ocean HC in the SCS was associated with strong climate anomaly occurring in the tropical region (**?**), and a high negative correlation occurred when the upper-ocean HC lags LST by ∼1–2 months (**?**).

Our analysis confirmed that the upper-ocean, average HC in the SCS was lower than normal (associated with shallower thermocline depth) during El Niño years, and vice versa during La Niña years. In terms of a heat capacitor, the SCS loses heat during the El Niño years, despite the enhanced surface heat flux (**?**). Some early studies, such as **?**, have suggested that the two typical El Niño events, the 1982/1983 and

[a]The objectively analyzed monthly mean temperatures data set was compiled by Ishii et al (2006, Version 6.2; Ishii06) at 16 levels (0 m, 10 m, 20 m, 30 m, 50 m, 75 m, 100 m, 125 m, 150 m, 200 m, 250 m, 300 m, 400 m, 500 m, 600 m, 700 m) for 1945–2005. The Ishii06 data set covers the global oceans with a horizontal resolution of 1°×1°.

[b]Assumed the sample number n=27, the critical t-test value t_α=2.052 when α=0.05, then the critical correlation coefficient $r_c = \sqrt{\frac{t_\alpha^2}{n-2+t_\alpha^2}} = 0.38$.

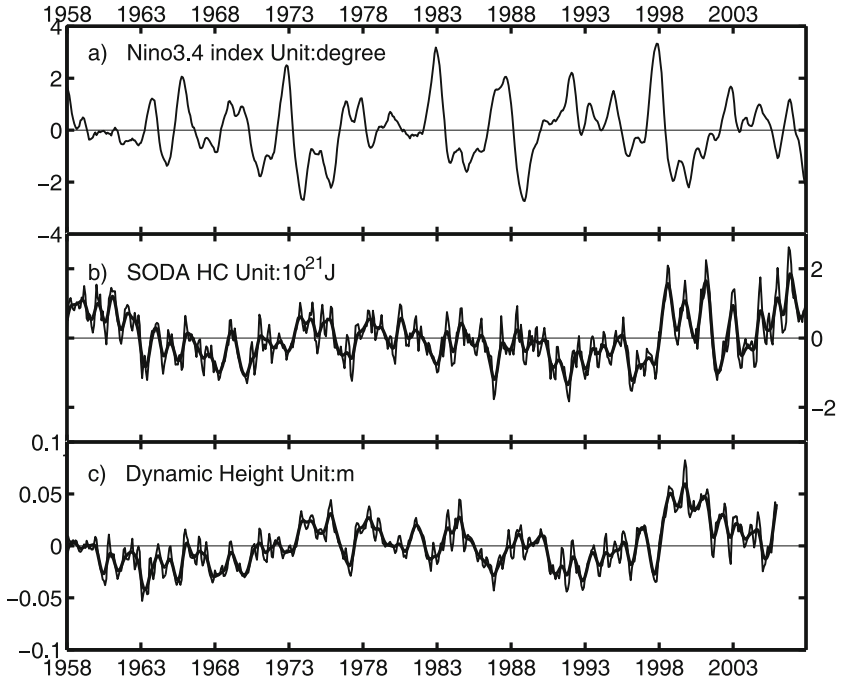

Fig. 1. (a) Raw time series (thin line) and the interannual signals (bold line) of the NINO3.4 index (°C), (b) domain-integrated SODA HC in upper 465 m (10^{21}J), and (c) domain-averaged DH (m) anomaly. The cubic smoothing spline was applied to extract the interannual variability of from the original time series.

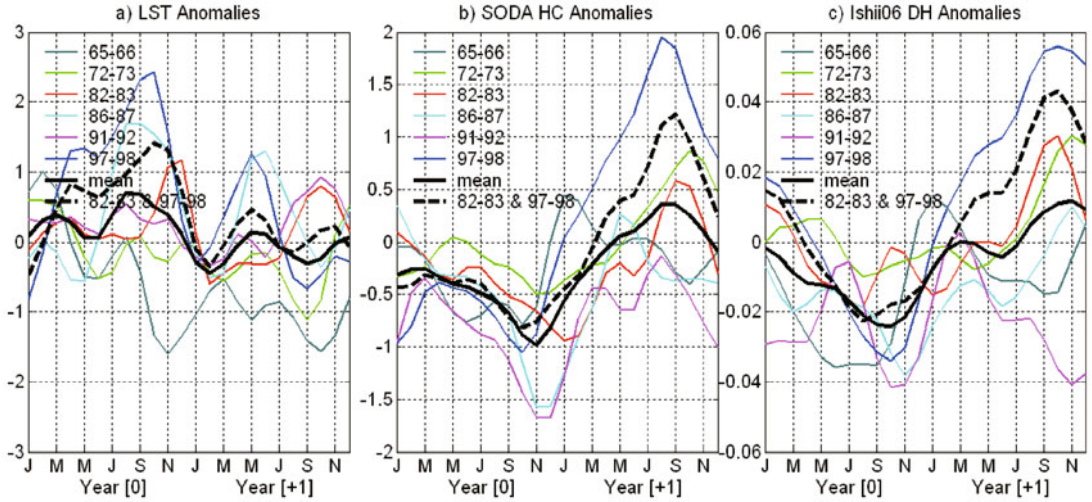

Fig. 2. Three-month running mean of LST, HC, and DH for the SCS: (a) SODA LST (Sv); (b) SODA HC (10^{21} J); (c) Ishii06 DH (m), with anomalies associated with six El Niño warm events during the El Niño year (year [0]) and the subsequent year of the El Niño year (year [+1]). The thick black real/dashed-curve represents the mean HC and DH anomalies for six El Niño events and two super-warm El Niño events.

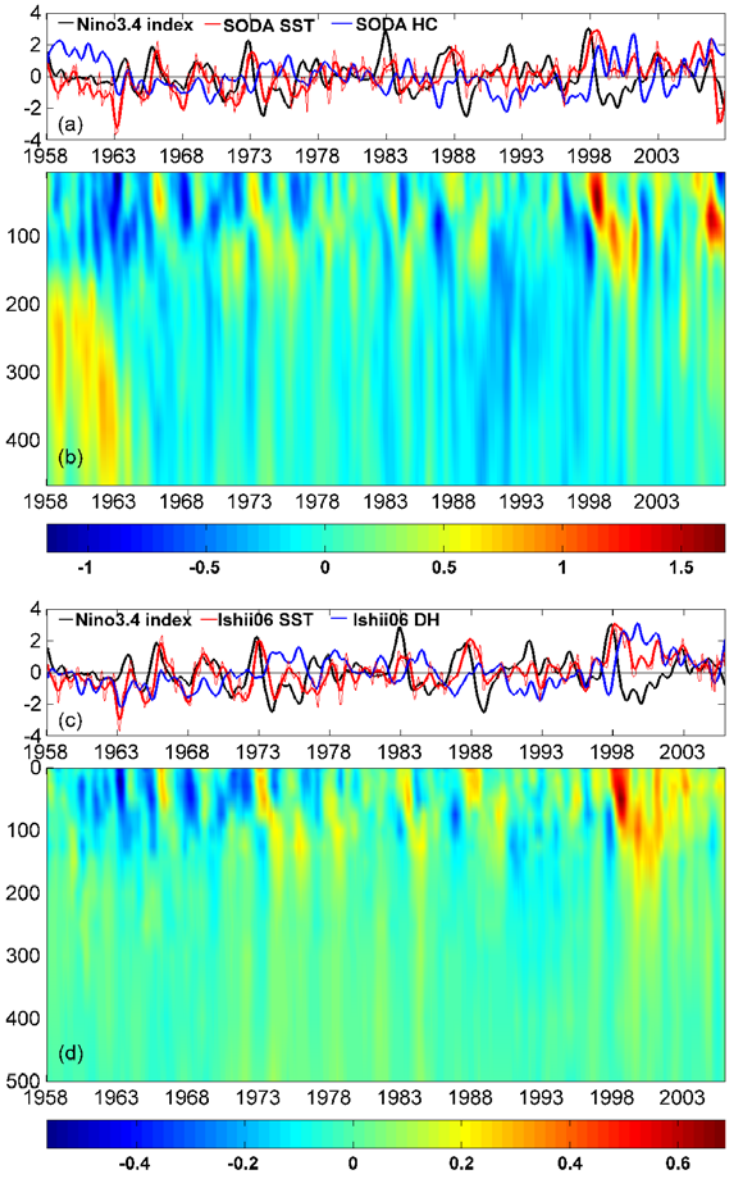

Fig. 3. Normalized interannual variability of the NINO3.4 index (black line): (a) SODA SST (red line), SODA HC (blue line); (c) Ishii05 SST (red line), Ishii06 DH (blue line) anomaly. The vertical profiles of temperature anomaly were domain averaged in the SCS from (b) SODA and (d) Ishii06 datasets, respectively.

the 1997/1998, are exceptions to this feature. However, our results show that this feature remained during these two typical El Niño events. That is to say, the upper-ocean HC was also lower than normal during the mature phases of the 1982/1983 and 1997/1998 events.

Applying the same method used by **?**, six significant El Niño warm events (i.e., 1965/1966, 1972/1973, 1982/1983, 1986/1987, 1991/1992, and 1997/1998) were chosen for the composite analysis. In the following analysis, [0] and [+1] denote the El Niño year and the subsequent year, respectively. Figure 2 displays the LST, SCS, HC, and DH anomalies associated with the six El Niño warm
events during year [0] and [+1]. The negative anomalies of HC and DH were the prominent features during the mature phases of El Niño years; they were associated with increasing LST (Fig. 2). The mean SCS

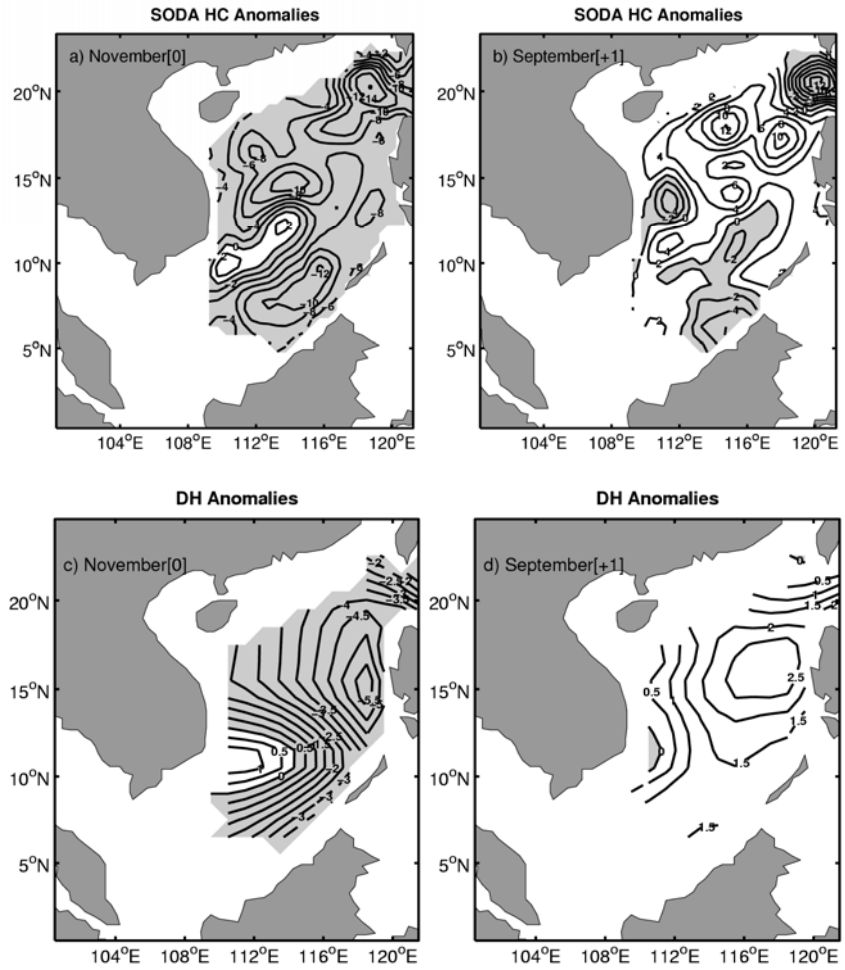

Fig. 4. Composites of the SODA heat storage anomalies (10^8 J m^{-2}) in (a) November [0], (b) September [+1]. The meanings of (c) and (d) are the same, except for Ishii06 DH anomalies (m). Negative values are shaded.

HC for six warm events shows that the cold anomaly peak occurred in November [0] and then shifted to the warm peak in September [+1] (Fig. 2b), and the interannual variability of the DH was similar to that of the HC (Fig. 2c). The double-peak of the HC occurring in March [+1] and September [+1] seems similar, with the double-peak evolutions of the SCS SST following an El Niño event, as reported by **?**.

This comparison demonstrates that the upper-ocean HC and the DH agree with each other very well; thus, we used the data assimilation products to study the interannual variability of the upper-ocean HC in the SCS to study vertical and horizontal thermal structures. During the El Niño events, especially in 1997/1998 events, the SST warmed more than normal (**?**), but the upper-ocean HC was lower than normal. What really drives such a lower-than-normal upper-ocean HC? Did the cooling role played by the SCSTF also occur during the 1982/1983 and 1997/1998 El Niño events? What about the thermocline variability? We studied the thermal structures in the upper-ocean (see sections 3.2 and 3.3), and our analysis focused on the upper-ocean heat budget (see section 3.4).

3.2 *Vertical thermal structures*

Figure 3 shows the SCS-averaged interannual variability of the SST anomaly and the vertical profile of temperature anomaly obtained from the SODA and Ishii06 data sets. The maximum correlation of 0.49 occurred when the NINO3.4 index led SODA SST for 5 months (Fig. 3a, black and red lines), and it reached 0.53 when the NINO3.4 index led the Ishii06 SSTs for 5 months (Fig. 3c, black and red lines). The physical processes responsible for the SCS interannual SST anomalies were investigated by **?** in detail.

The interannual variability of the upper-ocean HC was not in phase with the SST, and the maximal correlation coefficient was only 0.31 when SSTs led by 1

month, as inferred from the ocean model (Fig. 3a, red and blue lines), and the maximum correlation coefficient inferred from the Ishii06 data set was 0.46 when the SSTs led the DHs by 4 months (Fig. 3c, red and blue lines). Additional influence on the upper-ocean HC came from the subsurface temperature changes, especially in the thermocline depth. During El Niño events, the domain-averaged upper-ocean HC anomaly in the SCS was negative due to the cold anomalies that occurred in the thermocline depths (Figs. 3b and d). The response of SST and sea level in the SCS to ENSO was opposite, and the thermosteric sea level had an excellent correlation with subsurface temperature variation (**?**).

3.3 *Horizontal structures*

The composite fields of the heat storage and DH anomalies in November [0] and September [+1] (different stages of El Niño years) are shown in Fig. 4. The entire SCS, except off Vietnam, became cold anomalies in November during mature phases of El Niño events (Fig. 4a). The ambient cold anomalies were located north of the SCS (where the Kuroshio can intrude into the SCS through the Luzon Strait), off the coast of the Philippine Islands, centrally west of the SCS, and south of the SCS respectively. The DH anomalies behaved with a pattern similar to the upper-ocean heat storage anomalies at the same time, with a negative center off the coast of the Philippine Islands and a positive center off the coast of Vietnam (Fig. 4c).

In September [+1], the subsequent year of El Niño year, the upper-ocean heat storage anomalies in SCS became warmer in most regions of the SCS, which were associated with positive DHs anomalies (Figs. 4b and d). The DH anomalies became positive in the SCS, and the maximum positive center was located off the west coast of the Philippine Islands. The cold anomalies near the Luzon Strait and southwest of SCS were not restored to a normal state but only weakened in September [+1], and these finer characters can only be reflected from the ocean model with higher resolution, not from the objectively analyzed DH product.

3.4 *Processes generating the SCS HC anomalies*

The influence of ENSO can be transferred into the SCS through the atmospheric bridges, which can result in changes of surface wind, air temperature, humidity, and cloud amount that in turn influence surface heat fluxes and ocean circulations over other ocean basins (**?**; **?**). With the exception of the atmospheric bridge, LST can also play a role in conveying the impact of ENSO into the SCS, and the changes of the upper ocean HC in the SCS are mainly affected by horizontal advection directly linked to LST plus the air–sea heat flux (**?**). In this section, the roles played by the surface heat flux, ocean advection are discussed according to the conservation equation for heat integrated in the upper 465 m over the SCS.

Integrated over an enclosed box in the upper ocean, the conservation equation for heat was used (**?**):

$$
\begin{aligned}
c_p\rho \iiint\limits_{\text{box}} \frac{\partial \overline{T}}{\partial t} d\sigma = {} & \overline{Q_{\text{net}}} - c_p\rho \iint\limits_{A_\text{l}} \overline{v_\text{n}} \left(\overline{T} - T_0\right) dA - \\
& c_p\rho \iint\limits_{A_\text{b}} \overline{w} \left(\overline{T} - T_0\right) dA - \\
& c_p\rho \iint\limits_{A_\text{l}} \overline{v_\text{n}' T'} dA - c_p\rho \iint\limits_{A_\text{b}} \overline{w' T'} dA + \\
& c_p\rho \iint\limits_{A_\text{l}} K_h \frac{\partial}{\partial n} \left(\frac{\partial^2 \overline{T}}{\partial x^2} + \frac{\partial^2 \overline{T}}{\partial y^2} \right) dA + \\
& c_p\rho \iint\limits_{A_\text{b}} \overline{K_v \frac{\partial T}{\partial z}} dA
\end{aligned}
$$

where the independent variables x, y, and z are the eastward, northward, and vertical (upward) coordinates, respectively; t is time; dA is a two-dimensional element of area; and A_l and A_b are the later and lower boundary areas, respectively; $d\sigma$ is an element of volume. The over-bar represents the monthly mean. The prime denotes the disturbance term. T is the temperature; T_0 is the reference temperature chosen as zero conventionally; v_n is the horizontal velocity component normal to the lateral boundary; and w is the vertical velocity; and $c_p\rho$ is the specific heat capacity per unit volume.

The term on the left-hand side represents the rate of change of HC. The first term on the right-hand side is the net surface heat flux into the ocean; the second and third terms are the horizontal and vertical advection. The fourth and fifth terms represent the horizontal and vertical eddy heat fluxes resolved by the model on time scales less than 30 days (omitted here because SODA uses monthly time resolution). The last three terms are the parameterizations of horizontal and vertical diffusion associated with mixing, respectively, associated with sub-grid-scale processes,

[c]The original vertical diffusion of momentum was carried out using K-profile parameterization (KPP) mixing with modifications to address issues such as diurnal heating, while lateral subgrid-scale processes were modeled using biharmonic mixing (Carton et al., 2008). Only a rough estimation is given here due to a lack of information about SODA products. For simplicity, K_h and K_v

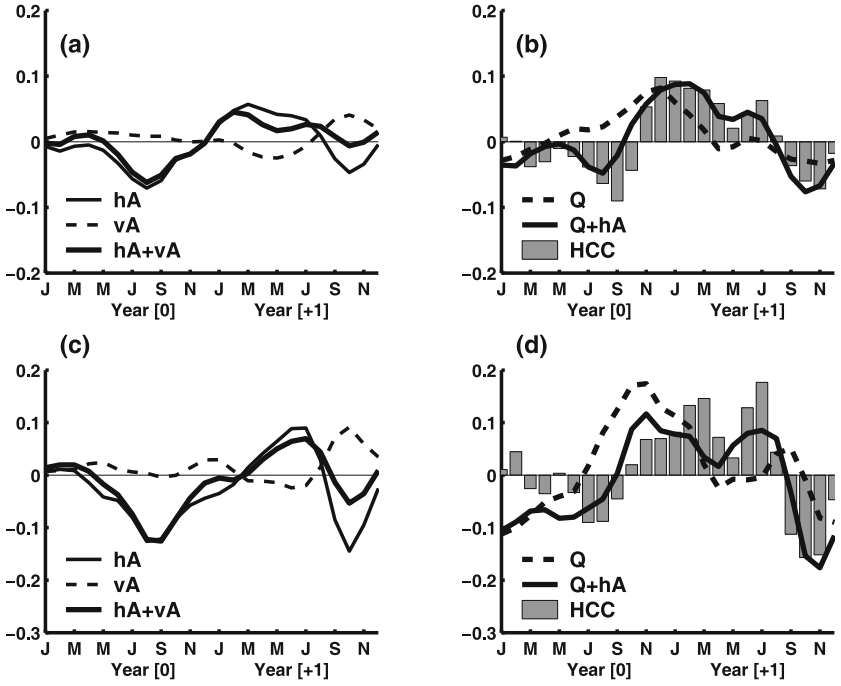

Fig. 5. Three-month running mean of (a) horizontal (solid curve), vertical (dashed curve), and total (bold solid curve) advections, and (b) ERA40 surface heat flux (dashed curve), surface heat flux plus horizontal advection (solid curve), and rate of change in HC in the upper 465 m of the SCS for six warm events (shadow). (c) and (d) are the same as (a) and (b) except for 1982/1983 and 1997/1998. Units: PW. Positive values indicate heat transfer into the SCS.

together calculated as the residual of the heat budget[c].

The composite analysis for six warm events showed that the variation of the vertical advection likely counterbalanced part of the effect of the horizontal advection, especially during the subsequent year of the El Niño year from March to November (Fig. 5a). Although the strength of vertical mixing can affect the deep-water overflow through the Luzon Strait, and thus contribute to the regulation of both heat flux and mass flux in the middle and upper part of the ocean (**?**), the role played by the vertical advection is small compared with the horizontal advection.

Figure 5b shows that the cooling advection attributed to the SCSTF was the key factor controlling the rate of the heat-content change in the upper 465 m during the El Niño years from July to November. During the decay of the El Niño events, the SCS warming was associated with increasing surface heat flux and the warming advection from January to September. The recent study showed that the tropical Indian Ocean sea-surface warming acts like a capacitor, anchoring atmospheric anomalies over the Indo-western Pacific Oceans (**?**). The summer warming anomalies of the SCS after El Niño may have been associated with the Indian Ocean capacitor effect.

The mean variation of advection during 1982/1983 and 1997/1998 events, and their relationship to surface fluxes and local changes in heat content in the SCS are also shown in Figs. 5c and d. These results show that the mean variation in the two super events was similar to that of the total composite analysis. The upper-ocean, average HC in the SCS declined during the mature phase of El Niño events and increased in the subsequent El Niño year. The SCS had a net heat gain from the atmosphere from January [0] to April [+1], thus the surface heat flux also cannot explain the decline of the HC that occurred during the mature phase of El Niño, which was mainly controlled by the horizontal advection associated with the SCSTF.

4. Summary and discussion

The interannual variability of the upper-ocean heat content anomalies in the SCS share the similar fea-

are the horizontal and vertical diffusion coefficients set to 500 $m^2\ s^{-1}$ and $5.0\times10^{-5}\ m^2\ s^{-1}$, respectively. The results show that the horizontal diffusion into the SCS through Luzon Strait was $\sim 1.85\times10^{12}$ W, and the vertical diffusion was about -4.73×10^{12} W, which was smaller than the advection [O(10^{13} W)] and is omitted in the discussion.

ture of DH anomalies, and both of them are connected with ENSO events. Associated with abnormal subsurface temperature cooling, the HC in the upper-ocean of the SCS was lower than normal during the mature phase of El Niño, which was mainly affected by the horizontal advection of the SCSTF, including those of the 1982/1983 and 1997/1998 events. After the low HC occurred during the mature phase of El Niño year, the high HC occurred during the subsequent year of El Niño year, which was mainly influenced by the net heat flux forcing.

Our analysis based on SODA products provides a good qualitative explanation for the abnormal cooling of the heat content in the upper 465 m in the SCS during the El Niño events, and the horizontal structure of the HC anomalies was complex, depending on the geophysical location. Thus, a better high-resolution model is needed to improve our understanding of ocean dynamics. The evolution of the HC in different geophysical regions may be regulated by different dynamic processes, which are worthy of further careful study.

Acknowledgements. This work was supported by the National Natural Science Foundation of China (Grant No. 40806005) and by the Chinese Academy of Sciences' Knowledge Innovation Program (Grant No. KZCX2-YW-Q11-02). The work described in this paper was also partially supported under the South China Sea Institute of Oceanology (Grant No. SQ200814). The authors are grateful to two anonymous reviewers for helpful comments that improved this manuscript.

REFERENCES

Carton, J. A., B. S. Giese, and S. A. Grodsky, 2005: Sea level rise and the warming of the oceans in the SODA ocean reanalysis. *J. Geophys. Res.*, **110**, 1–8.

Chu, P. C., N. L. Edmons, and C. W. Fan, 1999: Dynamical mechanisms for the South China Sea seasonal circulation and thermohaline variabilities. *J. Phys. Oceanogr.*, **29**, 2971–2989.

Fang, G. H., Z. X. Wei, B. H. Choi, K. Wang, Y. Fang, and W. Li, 2003: Interbasin freshwater, heat and salt transport through the boundaries of the East and South China Seas from a variable-grid global ocean circulation model. *Science in China* (*D*), **46**(1), 149–161.

Fang, G. H., D. Susanto, I. Soesilo, Q. A. Zheng, F. L. Qiao, and Z. X. Wei, 2005: A note on the South China Sea Interocean Circulation. *Adv. Atmos. Sci*, **22**(6), 946–954.

Fang, G. H., Y. G. Wang, Z. X. Wei, Y. Fang, F. L. Qiao, and X. M. Hu, 2009: Interocean circulation and heat and freshwater budgets of the South China Sea based on a numerical model. *Dyn. Atmos. Oceans*, **47**, 55–72.

He, Y. H., C. H. Guan, and Z. J. Gan, 1997: Interannual and interdecadal variations in heat content of the upper ocean of the South China Sea. *Adv. Atmos. Sci.*, **14**(2), 271–276.

Hu, J. Y., H. Kawamura, H. S. Hong, and Y. Q. Qi, 2000: A review on the currents in the South China Sea: Seasonal circulation, South China Sea Warm Current and Kuroshio intrusion. *J. Oceanogr.*, **56**, 607–624.

Ishii, M., M. Kimoto, K. Sakamoto, and S. I. Iwasaki, 2006: Steric sea level changes estimated from historical ocean subsurface temperature and salinity analyses. *J. Oceanogr.*, **62**, 155–170.

Klein, S. A., B. J. Soden, and N.-C. Lau, 1999: Remote sea surface temperature variations during ENSO: Evidence for a tropical atmospheric bridge. *J. Climate*, **12**, 917–932.

Lebedev, K. V., and M. I. Yaremchuk, 2000: A diagnostic study of the Indonesian Throughflow. *J Geophys Res.*, **105**(C5), 11243–11258.

Liu, Q. Y., R. X. Huang, D. Wang, Q. Xie, and Q. Z. Huang, 2006: Interplay between the Indonesian throughflow and the South China Sea throughflow. *Chinese Science Bulletin*, **51**, 50–58.

Liu, Q. Y., D. Wang, W. Zhou, Q. Xie, and Y. Zhang, 2010: Covariation of the Indonesian Throughflow and South China Sea Throughflow Associated with the 1976/77 Regime Shift. *Adv. Atmos. Sci*, **27**(1), 87–94, doi: 10.1007/s00376-009-8601-3.

Metzger, E. J., and H. E. Hurlburt, 1996: Coupled dynamics of the South China Sea, the Sulu Sea and the Pacific Ocean. *J. Geophys. Res.*, **101**(C5), 12331–12352.

Qu, T. D., G. Meyers, and J. S. Godfrey, 1994: Ocean dynamics in the region between Australia and Indonesia and its influence on the variation of sea surface temperature in a global general circulation model. *J. Geophys. Res.*, **99**(C9), 18433–18445.

Qu, T. D., Y. Y. Kim, and M. Yaremchuk, T. Tozuka, A. Ishida, and T. Yamagata, 2004: Can Luzon Strait transport play a role in conveying the impact of ENSO to the South China Sea? *J. Climate*, **17**, 3644–3657.

Qu, T. D., Y. Du, G. Meyers, A. Ishida, and D. X. Wang, 2005: Connecting the tropical Pacific with Indian Ocean through South China Sea. *Geophys. Res. Lett.*, **32**, L24609, doi: 10.1029/2005GL024698.

Qu, T. D., Y. Du, and H. Sasaki, 2006: South China Sea throughflow: A heat and freshwater conveyor. *Geophys. Res. Lett.*, **33**, L23617, doi: 10.1029/2006GL028350.

Qu, T. D., Y. T. Song, and T. Yamagata, 2009: An introduction to the South China Sea throughflow: Its dynamics, variability, and application for climate. *Dyn. Atmos. Oceans*, **47**, 3–14.

Rong, Z. R., Y. G. Liu, H. B. Zong, and Y. C. Cheng, 2007: Interannual sea level variability in the South China Sea and its response to ENSO. *Global Planet Change*, **55**, 257–272.

Tozuka, T., T. D. Qu, and T. Yamagata, 2007: Dramatic

impact of the South China Sea on the Indonesian Throughflow. *Geophys. Res. Lett.*, **34**, L12612, doi: 10.1029/2007GL030420.

Tozuka, T., T. D. Qu, Y. Masumoto, and T. Yamagata, 2009: Impact of the South China Sea throughflow on the seasonal and interannual variations of the Indonesian throughflow. *Dyn. Atmos. Oceans*, **47**, 73–85.

Wang, B., R. G. Wu, and X. H. Fu, 2000: Pacific-East Asian teleconnection: How does ENSO affect East Asian climate? *J. Climate*, **13**, 1517–1536.

Wang, C. Z., W. Q. Wang, D. X. Wang, and Q. Wang, 2006: Interannual variability of the South China Sea associated with El Niño. *J. Geophys. Res.*, **111**, C03023, doi: 10.1029/2005JC003333.

Wang, D. X., Q. Y. Liu, R. X. Huang, Y. Du, and T. D. Qu, 2006: Interannual variability of the South China Sea throughflow inferred from wind data and an ocean data assimilation product. *Geophys. Res. Lett.*, **33**, L14605, doi: 0.1029/2006GL026316.

Wang, W. W., Y. Q. Yu., C. Li., W. Zhou., Q. Y. Liu, and D. X. Wang, 2010: An investigation of the South China Sea throughflow and its impact on upper layer heat content of the South China Sea using LICOM. *Acta Oceanologica Sinica*, **32**(2), 1–11. (in Chinese)

Wang, W. W., D. X. Wang, W. Zhou, Q. Y. Liu, Y. Q. Yu, and C. Li., 2011: Impact of the South China Sea throughflow on the Pacific low-latitude western boundary current: A numerical study for seasonal and interannual timescales. *Adv. Atmos. Sci.* , **28**(6), 1367–1376, doi: 10.1007/s00376-011-0142-4.

Wyrtki, K., 1961: Physical oceanography of the Southeast Asian waters. Vol. 2, NAGA report, University of California, San Diego, 195pp.

Xie, S.-P., K. M. Hu, J. Hafner, H. Tokinaga, Y. Du, G. Huang, and T. Sampe, 2009: Indian Ocean capacitor effect on Indo-western Pacific climate during the summer following El Niño. *J. Climate*, **22**, 730–747.

Yaremchuk, M., J. McCreary, Z. J. Yu, and R. Furue, 2009: The South China Sea throughflow retrieved from climatological data. *J. Phys. Oceanogr.*, **39**, 753–767.

Yu, Z. J., S. Shen, J. P. McCreary, M. Yaremchuk, and R. Furue, 2007: South China Sea throughflow as evidenced by satellite images and numerical experiments. *Geophys. Res. Lett.*, **34**, L01601, doi: 10.1029/2006GL028103.

Yu, Z. J., J. P. McCreary, M. Yaremchuk, and R. Furue, 2008: Subsurface salinity balance in the South China Sea. *J. Phys. Oceanogr.*, **38**, 527–539.